

Nitrogen isotope stratigraphy of the Early Cambrian successions in the Tarim Basin: Spatial variability of nitrogen cycling and its implication for paleo-oceanic redox conditions

Bi Zhu¹ · Xuefeng Li¹ · Lu Ge¹ · Yongquan Chen²

Received: 12 January 2024 / Revised: 16 February 2024 / Accepted: 29 February 2024 / Published online: 25 April 2024
© The Author(s), under exclusive licence to Science Press and Institute of Geochemistry, CAS and Springer-Verlag GmbH Germany, part of Springer Nature 2024

Abstract The Early Cambrian represents a critical time period characterized by extraordinary biological innovations and dynamic redox conditions in seawaters. Nitrogen isotopic signatures of ancient sediments have the potential to elucidate the evolutionary path of marine redox states and the biogeochemical nitrogen cycle within the water column of the Early Cambrian ocean. While existing research on this topic has predominantly focused on South China, the exploration of other continental margins has been limited, leaving contradictory hypotheses untested. In this study, paired $\delta^{15}\text{N}$ and $\delta^{13}\text{C}_{\text{org}}$ analyses were performed on the Lower Cambrian successions from the Shairike section (inner ramp) and Well Tadong 2 (deep shelf/basin) in the northwestern and eastern Tarim Basin, respectively. Our data from the Shairike section reveal a discernible shift in the operation of different nitrogen cycles for the black chert-shale unit, also referred to as the black rock series in Chinese literature, of the Yurtus Formation (Fortunian stage to lower Stage 3). Oscillating $\delta^{15}\text{N}$ values for its lower part are suggestive of alternating anaerobic assimilation of NH_4^+ and denitrification/anammox. This is likely attributed to a shallow, unstable chemocline consistent with the upwelling and incursion of deep, anoxic waters during a major transgression. In contrast, aerobic nitrogen cycling, indicated by positive $\delta^{15}\text{N}$ values of >2‰, dominated the upper part alongside a reduction in upwelling intensity. On the other hand, the

$\delta^{15}\text{N}$ signatures of Xishanbulake and Xidashan Formations of Well Tadong 2, which encompass a time interval from the Cambrian Fortunian Age to Age 4, are indicative of N_2 fixation by diazotrophs as the major nitrogen source. The two studied intervals, although not time-equivalent, exhibit separated states of nitrogen cycling at least during the deposition of the Yurtus black rock series. The spatially different nitrogen cycling of the studied sections is compatible with a redox-stratified ocean during the deposition of the Yurtus black rock series. The build-up of a NO_3^- reservoir and aerobic nitrogen cycling in seawater was largely restricted to near-shore settings whereas anaerobic nitrogen cycling dominated by N_2 fixation served as the main nitrogen uptake pathway in off-shore settings.

Keywords Nitrogen isotopes · Early Cambrian · Tarim · Black rock series

1 Introduction

The Early Cambrian marks a unique time interval of remarkable biological innovation known as the “Cambrian explosion”, which is characterized by the rapid appearance of most phyla of modern animals and the development of a modern-like marine ecosystem (Sperling et al. 2013; Zhang and Shu 2014; Butterfield 2018). Although internal factors like genomic reorganization and ecological opportunities may have played crucial roles in triggering the biological event (Erwin et al. 2011; Mills and Canfield 2014; Butterfield 2018), the belief persists that profound changes in environmental conditions are closely associated with the diversity and decline of life during the Early Cambrian (e.g., Chen et al. 2015; He et al. 2019; Jin et al. 2016; Li et al. 2018; Wang et al. 2018a; Wei et al. 2018). One commonly

✉ Bi Zhu
zhubi@hhu.edu.cn

✉ Lu Ge
gelu211@163.com

¹ Institute of Earth’s Critical Zone, School of Earth Sciences and Engineering, Hohai University, Nanjing 210098, China

² Research Institute of Exploration and Development, Tarim Oil Field Company, PetroChina, Korla, China

cited key variable among the environmental factors is the oxygen concentration in the atmospheric-oceanic system. A rise in oxygen levels in seawater would facilitate biological innovation via producing more stable oxygenated habitats. Additionally, nutrient and food availability have also been considered as active players in early animal radiation (Cook and Shergold 1984; Brasier 1992; Sperling and Stockey 2018). The primary productivity of primary producers, which provide a fundamental food source for early animals, is ultimately regulated by nutrient availability in the ocean (Anbar and Knoll 2002; Knoll 2017). Consequently, great attention was paid to nutrient availability and its connection with macroevolution.

As a macronutrient, the availability of nitrogen in seawater is crucial for regulating primary productivity and shaping the marine ecosystem (Knoll and Follows 2016; Knoll 2017). Changes in nitrogen availability over geological time may have a profound influence on the evolution of eukaryotes (Stüeken et al. 2016; Wang et al. 2018a; Kipp et al. 2018). Due to the redox-sensitive nature of the biogeochemical cycle of nitrogen, the availabilities of different nitrogen species, such as NH_4^+ and NO_3^- in the water column, are strongly bonded to the seawater redox conditions (Stüeken et al. 2016). As fractionations of nitrogen isotopes via different metabolic pathways are variable, changes in the oceanic nitrogen cycle may potentially leave isotopic signatures in marine sedimentary records. For example, the prevalence of NH_4^+ assimilation by organisms tends to produce highly negative $\delta^{15}\text{N}$ values in marine sediments (e.g., Chen et al. 2019; Higgins et al. 2012; Xu et al. 2020), while highly positive $\delta^{15}\text{N}$ values are commonly associated with aerobic nitrogen cycles (Stüeken 2013; Cremonese et al. 2014; Ader et al. 2014; Wang et al. 2018a). Consequently, nitrogen isotope signatures in marine sediments have been used to assess the evolutionary path of marine redox states, the availability of different nitrogen species in seawater, as well as the biogeochemical nitrogen cycle within the water column in the geologic past (e.g., Ader et al. 2014; Boyle et al. 2013; Higgins et al. 2012; Koehler et al. 2017; Stüeken 2013; Stüeken et al. 2016; Wang et al. 2018b; Zerkle et al. 2008).

Given the vast potential of nitrogen isotopes in unveiling information on oceanic redox evolution and biological innovations, extensive investigation has been made on the $\delta^{15}\text{N}$ isotopic composition of Early Cambrian sedimentary successions (e.g., Chang et al. 2022, 2019; Chen et al. 2019; Cremonese et al. 2014; Wang et al. 2018a, 2015, 2021; Xiang et al. 2018; Xu et al. 2020; Zhang et al. 2017). These studies involving a variety of sedimentary facies have delineated a clearer picture of the oceanic nitrogen cycling during the Early Cambrian. However, debates still exist with respect to the role of fixed nitrogen supply in regulating animal radiations and declines (Chang et al. 2019; Xu et al. 2020). It has been hypothesized that the expansion of the oceanic

NO_3^- , along with the establishment of a modern-like aerobic nitrogen cycle, was related to the major waves of biological evolutions during the Ediacaran-Cambrian period (Wang et al. 2018a). However, a modern-like nitrogen cycle in a well-oxygenated ocean contradicts to the model of a redox-stratified ocean based on other geochemical indexes (e.g., trace elements, sulfur isotopes, Fe speciation) (Jin et al. 2016; Li et al. 2018, 2020). Up till now, most $\delta^{15}\text{N}$ data of this time interval were recovered from South China. In this case, data from more continental margins offer a perspective to test the different models and their implications in broader sense, and further, to achieve a better understanding of the global nitrogen cycle of the Early Cambrian ocean. Here we performed $\delta^{15}\text{N}$ and $\delta^{13}\text{C}_{\text{org}}$ analyses on the Lower Cambrian successions from the Shaijire section (inner ramp) and the Well Tadong 2 (deep shelf/basin) in northwestern and eastern Tarim Basin, respectively, with the aim to explore the pathways of nitrogen cycling and to unravel possible links between nitrogen availability, water-column redox during the Early Cambrian in the Tarim region.

2 Geological setting

The Tarim Block, one of the oldest continental blocks in China, was formed during the late Proterozoic (Cai et al. 2011). The Tarim Block was part of the Rodinia supercontinent during the Neoproterozoic and transitioned into a rifting stage along with the breakup of Rodinia in the late Ediacaran (Li et al. 2008; Zhang et al. 2013). The late Ediacaran-Early Cambrian represents a rift-drift transition phase of the Tarim block (Li and Powell 2001; Li et al. 2008). By the Early Cambrian, the Tarim Block has evolved into an epicontinental sea (Zhang et al. 2015). According to the paleogeographic reconstruction, the Tarim Basin exhibits a transition from ramp facies into deep shelfal/basinal facies from northwest to the east (Fig. 1).

Cambrian outcrops are mainly distributed in the Wushikeping area (northwestern margin of Tarim) and the Quruqtagh area (northeastern margin of Tarim). In the northwestern Tarim, the Lower Cambrian succession comprises the Yurtus Formation, the Xiaoerbulake Formation and the Wusonggeer Formation in ascending order. The Yurtus Formation is composed of bedded phosphatic chert and black shale in the lower and middle parts and dolomite at the top. The overlying Xiaoerbulake Formation consists of grey, granular, and algal dolomite, followed by the micritic dolomite of the Wusonggeer Formation. Previous paleontological studies have reported the presence of small shelly fossils (SSFs) and acritarch assemblage in the Yurtus Formation. The SSFs and the AHC acritarch assemblage in the basal, phosphatic chert of the Yurtus Formation has constrained the unit of Early Fortunian age, while SSFs in

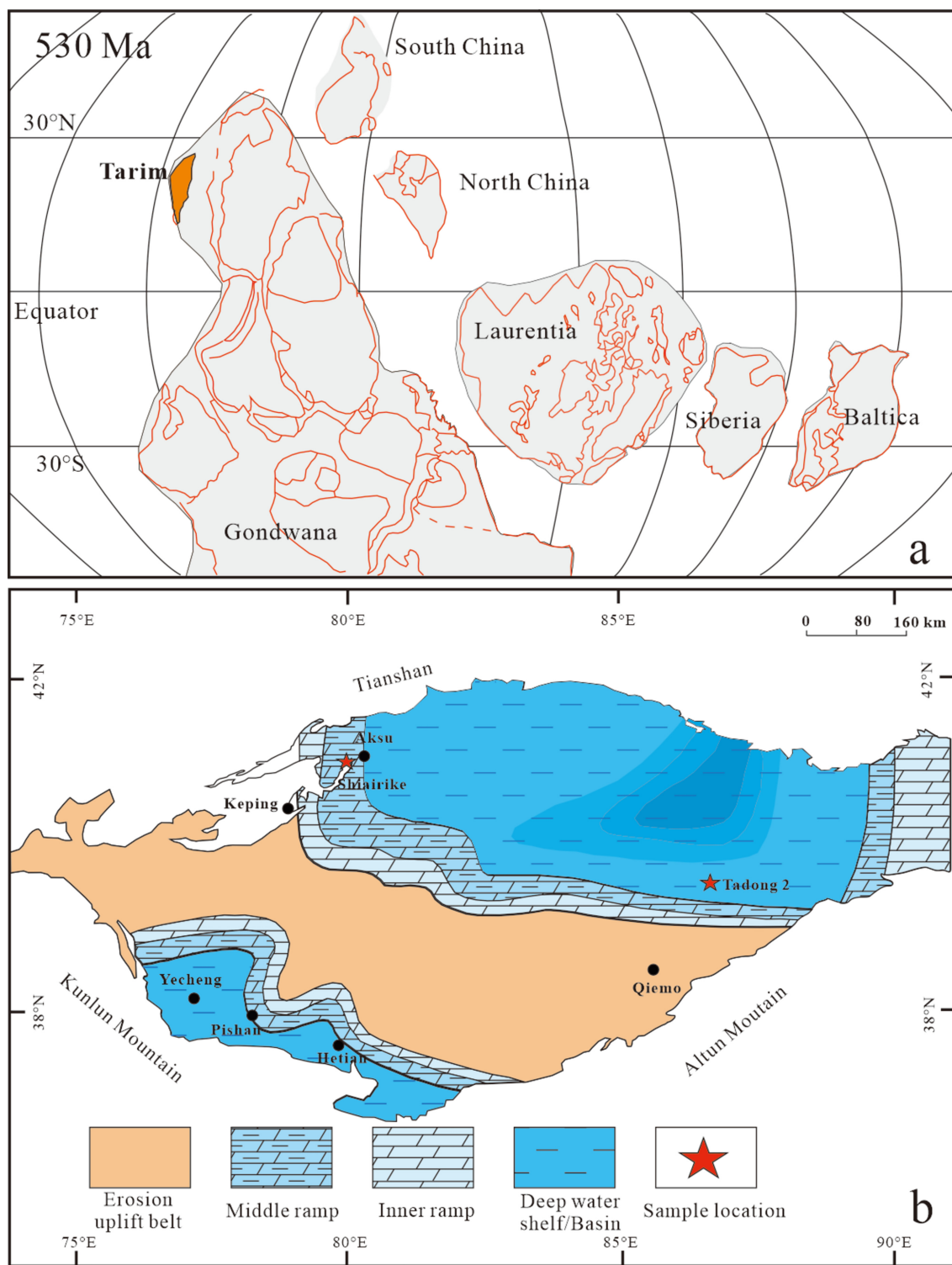


Fig. 1 **a** Global paleogeography of the Early Cambrian (after Li et al. 2008). **b** Paleogeography of the Tarim Basin during the Early Cambrian (after Tian et al. 2018)

the carbonates of the upper Yurtus Formation indicate this unit corresponds to the lower Chiungchussuan stage (Dong et al. 2009; Qian et al. 2009; Zhu et al. 2019). Moreover,

the overlying Xiaoerbulake Formation yields trilobite fossils typical of the Chiungchussuan stage (Zhou and Chen 1990; Peng et al 2012; Zhu et al 2019).

The Shairike section near the Aksu city is located within the inner ramp facies zone during the Early Cambrian (Fig. 1b). In this section, the basal Yurtus Formation is composed of grey, bedded chert with phosphatic nodules, followed by a black, organic-rich unit known as the black rock series in Chinese literature (e.g., Yu et al. 2003; Yang et al. 2017). This unit comprises thinly bedded cherts with intercalations of black shale for its lower part and mainly black shale for the upper part. Medium-thick bedded dolomite dominates the upper Yurtus Formation, which is overlaid by thickly bedded dolomite of the Xiaoerbulake Formation. 24 samples were collected from the lower part and 11 black shales were collected from the upper part (Fig. 2a; Table 1).

At the outcrops of the Quruqtagh area in the eastern Tarim Basin, the Lower Cambrian succession comprises the Xishanbulake Formation and the Xidashan Formation in ascending order. Generally, the Xishanbulake Formation is dominated by dark cherts with phosphatic chert developed at its base. The Xidashan Formation is composed mainly of carbonates with interlayers of shale and mudstone. The basal part of the Xishanbulake Formation yields AHC acritarch assemblage and *Kaiyangites* (Yao et al. 2005; Dong et al. 2009), indicating it is of Early Fortunian age. The upper part of this formation yields brachiopods (Zhou 2001) and the overlying Xishanbulake Formation yields abundant trilobites, archaeocyathids, brachiopod *Lingulella* and sponge spicules (Zhang et al. 1983; Zhu and Lin 1983; Zhong and Hao 1990; Peng et al. 2012). Collectively, the paleontological data indicate the upper part of the Xishanbulake Formation and the Xishanbulake Formation can be correlated with the Early Chiungchussuan Stage and Chiungchussuan-Duyunian Stage, respectively (Zhu et al. 2019; 2021).

Well Tadong 2 is located within the deep shelfal/basinal facies (Fig. 1b). The well was originally drilled for gas and petroleum exploration with a total depth of over 5000 m. Based on gamma (GR) values and lithostratigraphic features, the Lower Cambrian Xishanbulake and the Xidashan Formations cover a depth range from 4974 to 4887 m (Wang et al. 2022). The subdivision of the two formations within this interval remains controversial. The boundary of the two formations was proposed to be located at 4949 m (Cai et al. 2014) or 4920 m (Wang et al. 2022) (Fig. 2b). In the present study, we adopted the first subdivision framework, as the different subdivisions can not influence our data interpretation (see Sect. 5). Differing from the outcrop sections in the Kuluketage region, the Xishanbulake Formation in Well Tadong 2 is characterized by black shale with interlayers of argillaceous limestone (Fig. 2b). The Xidashan Formation is composed of calcareous black shale with intercalation of argillaceous limestone (Fig. 2b). Drill cuttings samples were collected from the well, including 8 from the Xishanbulake Formation and 32 samples from the Xidashan Formation (Table 2; Fig. 2b).

3 Analytical methods

Before chemical analysis, all samples were crushed to small chips. After a careful examination to avoid weathered surfaces and veins, the chips were cleaned using distilled water and then ground into powders (<200 mesh).

Organic carbon isotopic ratios measurement was performed at the Nanjing Institute of Geology and Palaeontology, Chinese Academy of Sciences. Prior to analysis, sample powders were treated using 2 N HCl for 24 h. The step was repeated until all the carbonate fractions in the sample powders were removed. The residue was then rinsed using Milli-Q water several times and dried in an oven. Afterward, the carbonate-free sample powders were wrapped in a tin capsule. The carbon isotopic ratios measurement was carried out using a Delta V mass spectrometer coupled to a Flash Elemental Analyzer. Carbon isotope values are reported in per mil (‰) relative to the Vienna Pee Dee Belemnite (VPDB). During analysis, USGS40 and UREA were used as standards for data calibration. Analytical error is within 0.5‰.

Total nitrogen (TN) and nitrogen isotopic ratio measurements were performed at the Beijing Createch Testing Technology Co. Ltd. Prior to analysis, each sample was decarbonated following the procedure described above for organic carbon isotopic analysis. The nitrogen isotopic ratios were measured on a MAT 253 plus mass spectrometer coupled to a Flash Elemental Analyzer via a Conflo IV interface. The standard B2151 was used for calibration and USG 588 was used for monitoring during the whole run. The δ¹⁵N values are reported relative to air with analytical error within 0.5‰. TN contents were obtained during isotopic measurements from the nitrogen plot area.

Total organic carbon (TOC) was analyzed at the Analytik Jena AG (Shanghai) Co. Ltd. The analysis was performed using an element analyzer (multi N/C 3100). Total organic carbon (TC) and total inorganic carbon were measured respectively, and TOC values were obtained by subtraction of total inorganic carbon (TIC) from TC.

Potassium content analysis for samples in the Shairike section was made at the ALS Chemex (Guangzhou) Co., Ltd. The analysis was performed using a ME-XRF26d by the melting film method, calibrated against international standards. The precision was better than 5%. Potassium content analysis of samples from the Well Tadong 2 was made at the Nanjing FocuMS Technology Co., Ltd. Samples powders were digested using mixed concentrated HNO₃ and HF following the method of Gao et al. (2003). The solution was then diluted and spiked with Rh. The measurement was performed on an ICP-OES (Agilent 5110) with an analytical precision of better than 5%.

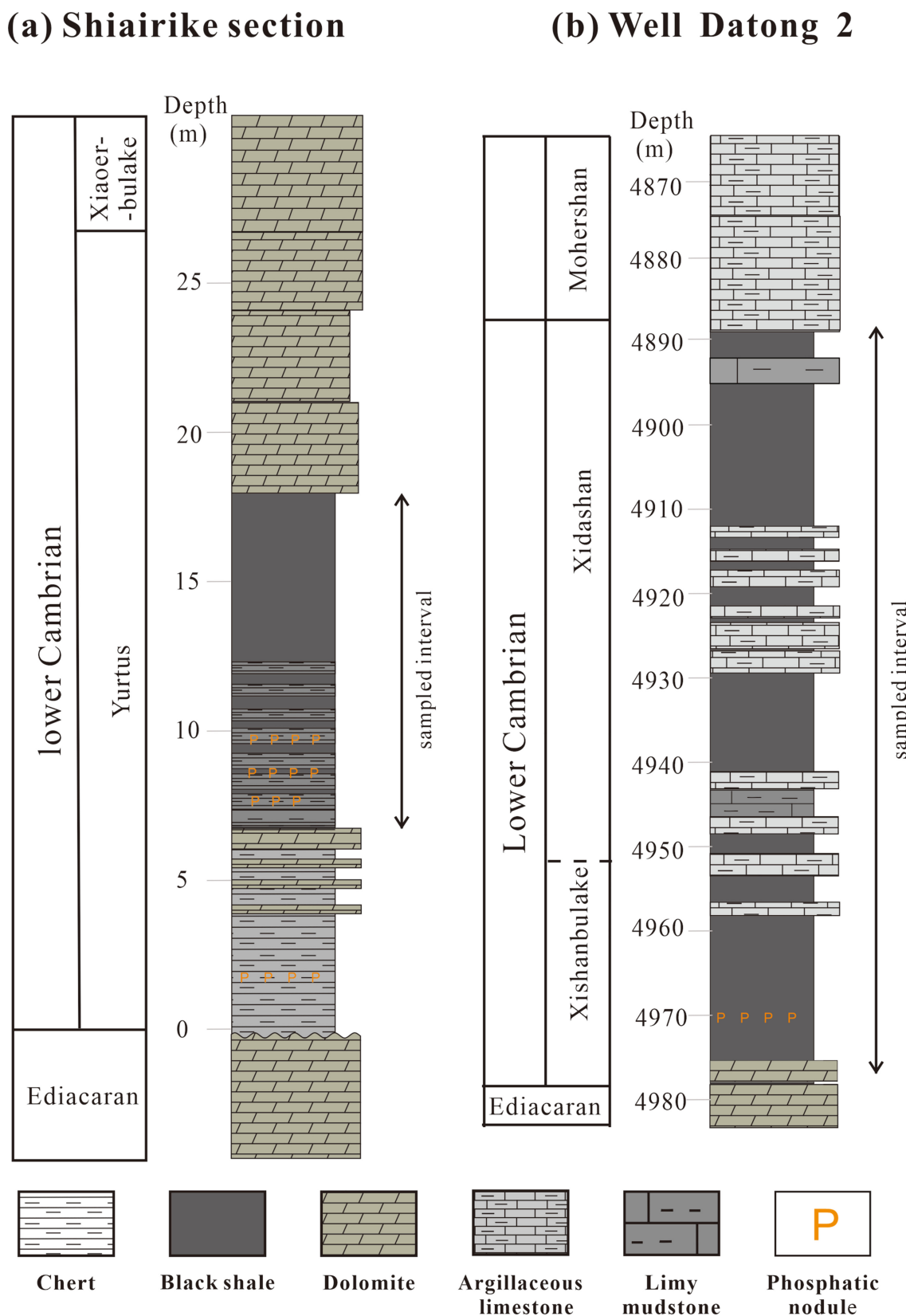


Fig. 2 **a** Lithological column of the Yurtus Formation in the Shairike section. **b** Lithological column of the Xishabulake and Xidashan Formations in Well Tadong 2

Table 1 Analytical results of $\delta^{15}\text{N}$, TN, $\delta^{13}\text{C}_{\text{org}}$, TOC and K_2O of samples from the Shairike section

Sample	lithology	Depth (m)	$\delta^{15}\text{N}(\text{\textperthousand})$	TN (%)	$\delta^{13}\text{C}_{\text{org}}(\text{\textperthousand})$	TOC (%)	C/N	$\text{K}_2\text{O} (\text{\textperthousand})$
SA-Y2-1	Argillaceous dolomite	6.6	4.2	0.06	-37.0	0.81*	16.1	0.04
SA-Y2-2	Phosphorites	6.8	3.8	0.05	-37.1	0.87*	21.5	0.34
SA-Y2-3	Chert	6.8	-0.9	0.21	-37.0	1.64*	8.9	
SA-Y2-5	Chert	7.1	1.3	0.05	-37.5	0.72	17.2	0.16
SA-Y2-6	Chert	7.2	1.4	0.06	-36.1	0.84	16.4	0.26
SA-Y2-8	Chert	7.9	-6.3	0.12	-36.5	3.24	32.4	0.08
SA-Y2-10	Chert	8.3	-1.7	0.03	-32.1	0.15	6.9	0.1
SA-Y2-11	Chert	8.5	-0.7	0.04	-34.9	0.42	13.2	0.12
SA-Y2-12	Chert	8.7	1.7	0.05	-36.2	1.52	32.5	0.14
SA-Y2-13	Phosphorites	8.9	1.0	0.05	-36.1	1.16*	28.7	0.22
SA-Y2-14	Phosphorites	9.0	3.5	0.41	-35.1	7.06*	20.1	0.63
SA-Y2-15	Chert	9.2	-1.9	0.05	-35.2	0.80	18.5	0.1
SA-Y2-16	Chert	9.4	0.6	0.05	-35.8	1.29	29.0	0.09
SA-Y2-17	Chert	9.6	-3.4	0.04	-34.7	0.57	15.8	0.06
SA-Y2-18	Chert	9.8	-3.3	0.04	-35.2	0.50	15.6	0.09
SA-Y2-19	Chert	10.0	-0.3	0.08	-34.7	3.17	45.1	0.08
SA-Y2-20	Chert	10.2	-4.9	0.04	-34.2	0.50	15.1	0.05
SA-Y2-21	Chert	10.4	-3.5	0.03	-32.8	0.19	6.4	0.11
SA-Y2-22	Chert	10.6	1.0	0.05	-34.2	1.38	34.3	0.07
SA-Y2-23	Chert	10.8	3.3	0.07	-34.4	1.31	20.4	0.17
SA-Y2-24	Chert	11.0	0.1	0.04	-31.8	0.37	10.9	0.16
SA-Y2-25	Chert	11.2	-2.8	0.06	-34.9	1.22	24.9	0.45
SA-Y2-26	Chert	11.4	1.9	0.04	-33.9	0.34	10.3	0.12
SA-Y2-27	Chert	11.7	0.2	0.07	-35.0	1.66	26.5	0.19
SA-Y3-1	Black shale	12.2	3.4	0.35	-34.9	13.39	45.0	1.96
SA-Y3-2	Black shale	12.4	3.0	0.27	-35.3	11.95	51.6	1.75
SA-Y3-3	Black shale	12.6	3.8	0.38	-35.0	12.49	38.0	1.67
SA-Y3-4	Black shale	12.9	3.5	0.34	-35.3	11.57	39.8	2.74
SA-Y3-5	Black shale	13.1	4.1	0.31	-35.0	9.18	34.8	1.39
SA-Y3-6	Black shale	13.3	2.5	0.35	-35.0	12.23	40.5	1.48
SA-Y3-7	Black shale	13.5	4.1	0.40	-34.8	11.73	34.1	2.53
SA-Y3-8	Black shale	13.8	1.6	0.45	-35.0	13.56	34.9	2.38
SA-Y3-9	Black shale	14.3	3.2	0.33	-35.2	10.66	37.5	1.39
SA-Y3-10	Black shale	15.8	1.4	0.34	-35.4	11.41	39.0	4.12
SA-Y3-11	Black shale	16.3	-1.3	0.34	-35.9	6.76	23.2	1.44

*TOC data from this study, other TOC data were from Zhu et al. (2022a)

4 Results

The obtained TOC, TN, $\delta^{13}\text{C}_{\text{org}}$, $\delta^{15}\text{N}$, and K_2O data are listed in Tables 1 and 2 and the vertical variations of studied intervals in the Shairike section and Well Tadong 2 are displayed in Figs. 3 and 4.

4.1 The Shairike section (northwestern Tarim)

The sampled interval at the Shairike section exhibits highly variable $\delta^{15}\text{N}$ values ranging from $-6.3\text{\textperthousand}$ to $4.2\text{\textperthousand}$ with an average of $0.7\text{\textperthousand}$. The lower, chert-dominant part

(LU) shows more variabilities ($-6.3\text{\textperthousand}$ to $4.2\text{\textperthousand}$, average = $-0.2\text{\textperthousand}$), with two pronounced negative excursions (Fig. 3). Comparably, $\delta^{15}\text{N}$ variations in the upper, black shale-dominating part (UU) are more limited ($-1.3\text{\textperthousand}$ to $4.1\text{\textperthousand}$), with a higher average value of $2.7\text{\textperthousand}$. The $\delta^{15}\text{N}$ stays positive through most of the interval with a shift towards negative values at the top (Fig. 3).

The $\delta^{13}\text{C}_{\text{org}}$ values range from $-37.5\text{\textperthousand}$ to $-31.8\text{\textperthousand}$ (average = $-35.1\text{\textperthousand}$). Like the $\delta^{15}\text{N}$ pattern, $\delta^{13}\text{C}_{\text{org}}$ values of the LU show more variability ($-37.5\text{\textperthousand}$ to $-31.8\text{\textperthousand}$, average = $-35.1\text{\textperthousand}$). The lower part of LU exhibits an overall positive excursion, with $\delta^{13}\text{C}_{\text{org}}$ value increasing

Table 2 Analytical results of $\delta^{15}\text{N}$, TN, $\delta^{13}\text{C}_{\text{org}}$, TOC and K_2O of samples from the Tadong 2 well

Sample	lithology	Depth (m)	$\delta^{15}\text{N}(\text{\textperthousand})$	TN (%)	$\delta^{13}\text{C}_{\text{org}}(\text{\textperthousand})$	TOC (%) ^a	C/N	$\text{K}_2\text{O} (\text{\textperthousand})$
<i>Xidashan Formation</i>								
TD-40	Argillaceous limestone	4887	0.0	0.03	-28.8	0.47	16.9	0.96
TD-39	Black shale	4889	-1.0	0.11	-29.3	1.72	18.0	3.94
TD-38	Black shale	4891	-0.9	0.11	-29.6	1.97	20.9	3.13
TD-37	Black shale	4893	-1.2	0.09	-29.6	1.80	22.7	2.60
TD-36	Black shale	4895	-1.6	0.09	-29.2	1.46	19.8	2.95
TD-35	Black shale	4897	-1.3	0.09	-29.4	2.01	24.7	2.90
TD-34	Black shale	4898	-1.3	0.08	-29.4	1.93	27.4	2.63
TD-33	Black shale	4901	-1.9	0.07	-29.6	2.20	35.7	2.38
TD-32	Black shale	4903	-1.1	0.10	-29.6	2.29	27.9	3.06
TD-31	Black shale	4905	-1.7	0.09	-29.9	2.43	31.6	2.78
TD-30	Calcareous black shale	4907	-1.4	0.05	-29.7	1.18	29.4	1.60
TD-29	Argillaceous limestone	4909	-0.5	0.03	-29.9	0.84	36.4	0.74
TD-28	Argillaceous limestone	4911	-0.7	0.03	-29.7	0.72	29.8	0.89
TD-27	Argillaceous limestone	4912	-0.3	0.03	-29.8	0.73	30.8	0.80
TD-26	Calcareous black shale	4914	-1.3	0.03	-30.1	1.13	39.4	0.75
TD-25	Black shale	4917	-1.7	0.05	-29.9	1.50	37.3	1.59
TD-24	Calcareous black shale	4919	-0.8	0.04	-30.1	1.30	42.5	0.77
TD-23	Calcareous black shale	4921	0.9	0.03	-29.7	0.92	30.6	0.89
TD-22	Calcareous black shale	4924	-0.2	0.04	-29.8	1.34	43.1	1.14
TD-21	Black shale	4925	-1.6	0.05	-30.0	1.53	33.6	1.64
TD-20	Black shale	4927	-0.8	0.06	-29.6	1.25	23.3	1.85
TD-19	Black shale	4928	-0.6	0.08	-29.8	1.42	21.7	2.23
TD-18	Black shale	4931	-1.6	0.08	-30.1	1.58	24.2	2.46
TD-17	Black shale	4933	-1.9	0.06	-30.2	2.09	38.7	1.37
TD-16	Calcareous black shale	4935	-1.1	0.04	-30.2	1.11	31.1	1.17
TD-15	Black shale	4937	-1.5	0.05	-29.9	1.21	28.7	1.47
TD-14	Black shale	4939	-1.2	0.05	-30.1	1.36	33.5	1.33
TD-13	Black shale	4941	-1.0	0.05	-30.1	1.58	40.2	1.39
TD-12	Black shale	4943	-0.3	0.04	-29.8	1.02	32.6	1.03
TD-11	Argillaceous limestone	4945	0.1	0.03	-29.6	0.78	28.9	0.89
TD-10	Argillaceous limestone	4947	0.9	0.03	-29.5	0.52	21.5	0.66
TD-9	Calcareous black shale	4949	-0.1	0.05	-29.7	1.16	29.8	1.43
<i>Xishanbulake Formation</i>								
TD-8	Black shale	4951	-0.8	0.06	-29.7	1.57	29.2	2.02
TD-7	Black shale	4956	0.0	0.07	-27.7	2.15	34.2	3.14
TD-6	Black shale	4959	-0.3	0.13	-30.7	4.47	38.7	5.36
TD-5	Black shale	4960	-0.7	0.18	-30.9	10.21	66.4	4.06
TD-4	Black shale	4961	-1.3	0.16	-31.7	9.06	67.6	3.46
TD-3	Black shale	4963	-1.1	0.09	-32.0	6.99	93.6	3.38
TD-2	Black shale	4965	-1.6	0.10	-32.3	6.06	73.9	3.59
TD-1	Calcareous black shale	4969	0.1	0.02	-31.3	0.44	24.4	1.11

^a data source: Guo et al. (2023)

from ca. -37.0 ‰ to ca. -32.0 ‰ before decreasing to ca. -36.0‰. The upper part of LU shows a gentler positive excursion ranging from ca. -35.0‰ to ca. -32.0‰. In contrast, the UU is characterized by slightly lower and more stable $\delta^{13}\text{C}_{\text{org}}$ values ranging from -35.9‰ to -34.8‰ (Table 1; Fig. 3).

TN ranges from 0.03% to 0.45% in this interval. The TN values for the LU (0.03% to 0.41%) are lower than the UU (0.27% to 0.45%), with average values of 0.07% and 0.35%, respectively. The vertical C/N pattern is similar to that of TN, with higher C/N for the UU (23.2 To 51.6, average=38.0) than the LU (6.4 To 45.1, average=20.3).

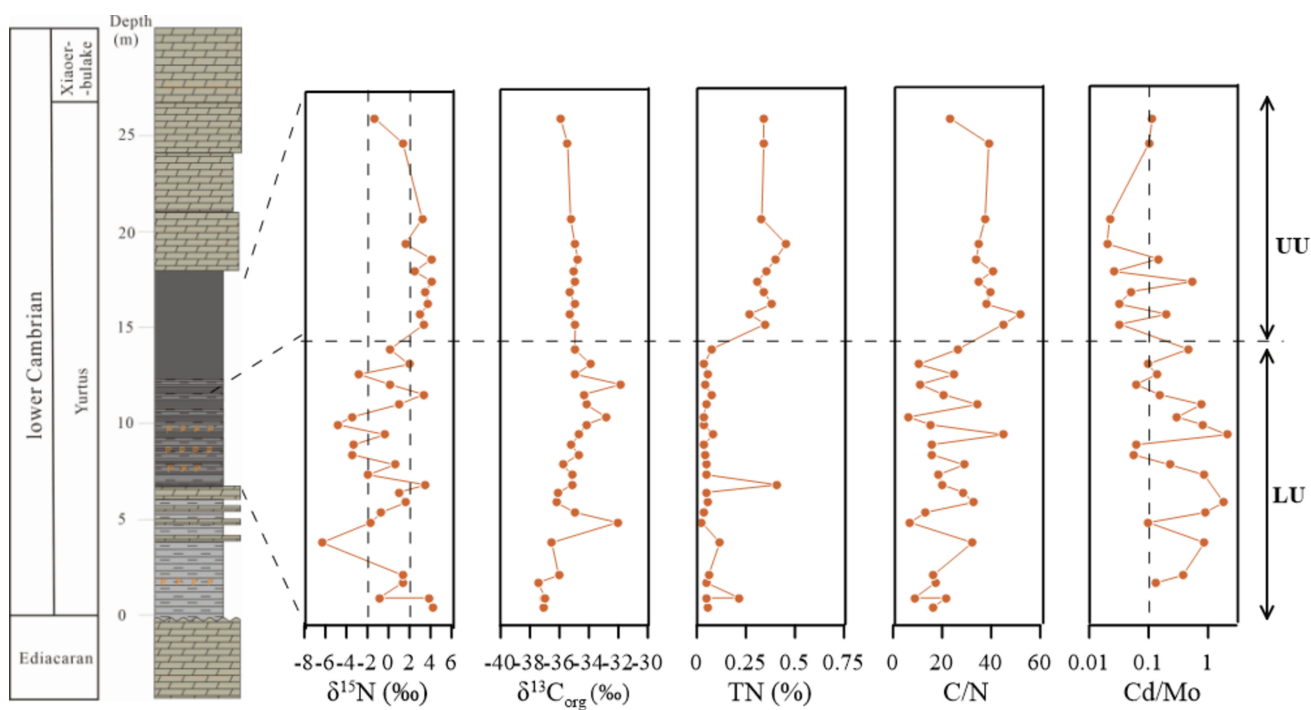


Fig. 3 Chemostratigraphic column of Yurtus Formation in the Shairike section. Cd/Mo data are from Zhu et al. (2022a)

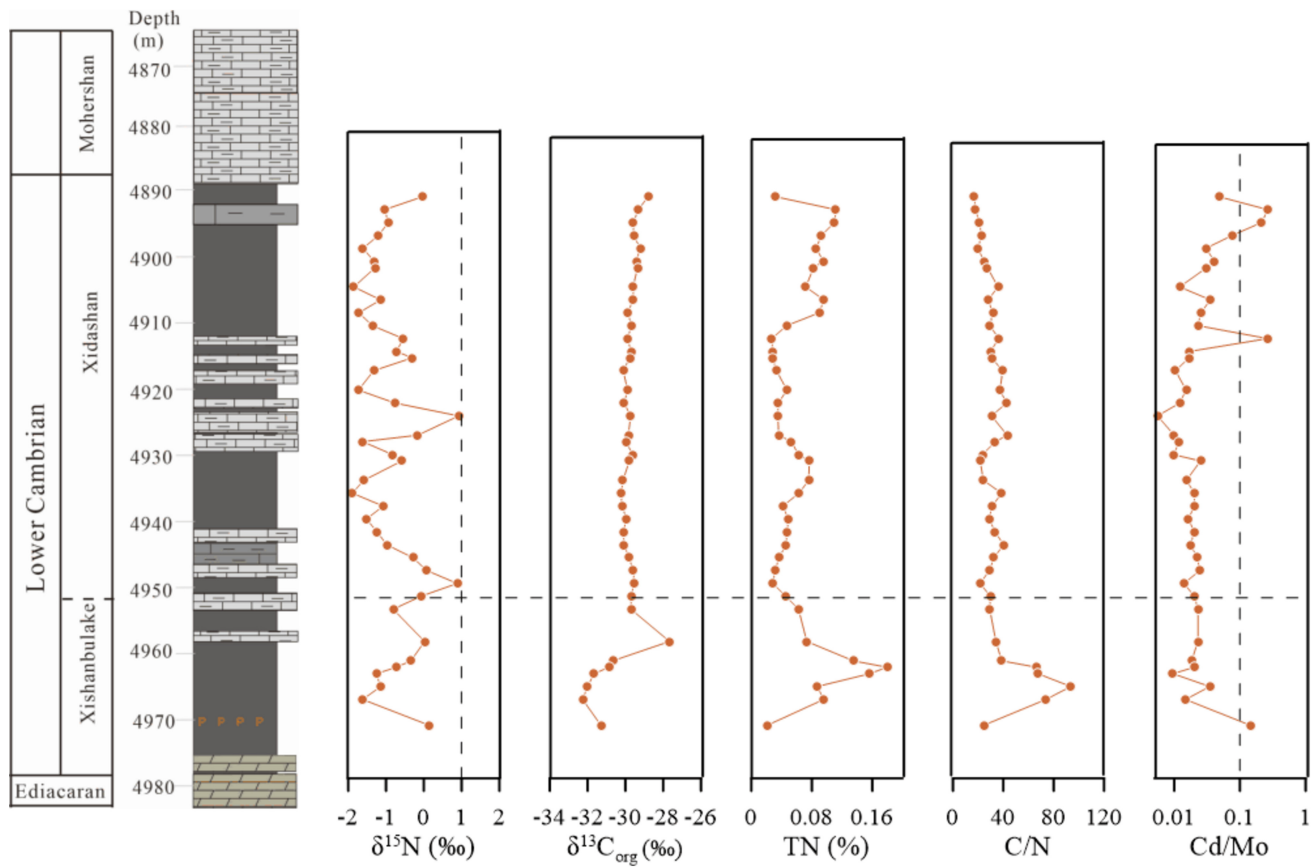


Fig. 4 Chemostratigraphic column of the Xishabulake and Xidashan Formations in Well Tadong 2. Cd/Mo data are from Guo et al. (2023)

4.2 Well Tadong 2 (eastern Tarim)

Overall, the $\delta^{15}\text{N}$ values for the Xishanbulake and Xidashan Formations exhibit limited variations, with all data within the range of $-2\text{\textperthousand}$ to 1\textperthousand (Table 2, Fig. 4). For the Xishanbulake Formation, the $\delta^{15}\text{N}$ ranges from $-1.6\text{\textperthousand}$ to $0.1\text{\textperthousand}$ (average = $-0.7\text{\textperthousand}$), with a small negative excursion at ca. 4960 m. The $\delta^{15}\text{N}$ values for overlying Xidashan Formation are broadly similar to that of the Xishanbulake Formation, ranging from $-1.9\text{\textperthousand}$ to $0.9\text{\textperthousand}$ (average = $-0.9\text{\textperthousand}$). Two small shifts towards more negative values can be observed in this formation, with nadirs of $-1.6\text{\textperthousand}$ and $-1.9\text{\textperthousand}$, respectively (Fig. 4).

The $\delta^{13}\text{C}_{\text{org}}$ values range from $-32.3\text{\textperthousand}$ to $-27.7\text{\textperthousand}$ (average = $-30.8\text{\textperthousand}$) for the Xishanbulake Formation, exhibiting a small negative excursion in the lower part with a nadir of $-32.3\text{\textperthousand}$ (Fig. 4). The $\delta^{13}\text{C}_{\text{org}}$ values then stabilize at ca. $30.0\text{\textperthousand}$ at the upper Xishanbulake Formation. The Xidashan Formation exhibit rather stable $\delta^{13}\text{C}_{\text{org}}$ values ranging from $-30.2\text{\textperthousand}$ to $-28.8\text{\textperthousand}$ (average = $-29.7\text{\textperthousand}$) (Table 2; Fig. 4).

The TN and C/N patterns for the Xishanbulake and Xidashan Formations are similar, with lower values for the latter. The TN and C/N of the Xishanbulake Formation vary from 0.02% to 0.18% (average = 0.10%) and 24.4 to

93.6 (average = 53.5), respectively. For the Xidashan Formation, the TN and C/N vary from 0.03% to 0.11% (average = 0.06%) and 16.9 to 43.1 (average = 29.8), respectively (Table 2; Fig. 4).

5 Discussion

5.1 Evaluation of carbon and nitrogen isotopic data

The $\delta^{13}\text{C}_{\text{org}}$ values of all the studied units fall within the range of typical Cambrian sedimentary successions in previous studies (e.g., Wang et al. 2015; Chang et al. 2019; Xu et al. 2020). None of the studied units exhibits significant correlations between TOC and $\delta^{13}\text{C}_{\text{org}}$ values (Figs. 5a, 6a), suggesting the remineralization of organic matter during diagenesis exerted only a limited influence on the primary $\delta^{13}\text{C}_{\text{org}}$ values. Nitrogen in sediments occurs as organic-bound nitrogen and clay-bound nitrogen, with the latter being an additional variable in regulating the bulk $\delta^{15}\text{N}$ values (Ader et al. 2016; Stüeken et al. 2016). For samples in the present study, linear correlations are observed in the TOC vs. TN cross plot for the Yurtus Formation at Shairike (Fig. 5b). Similarly, the TOC-TN cross plots exhibit good

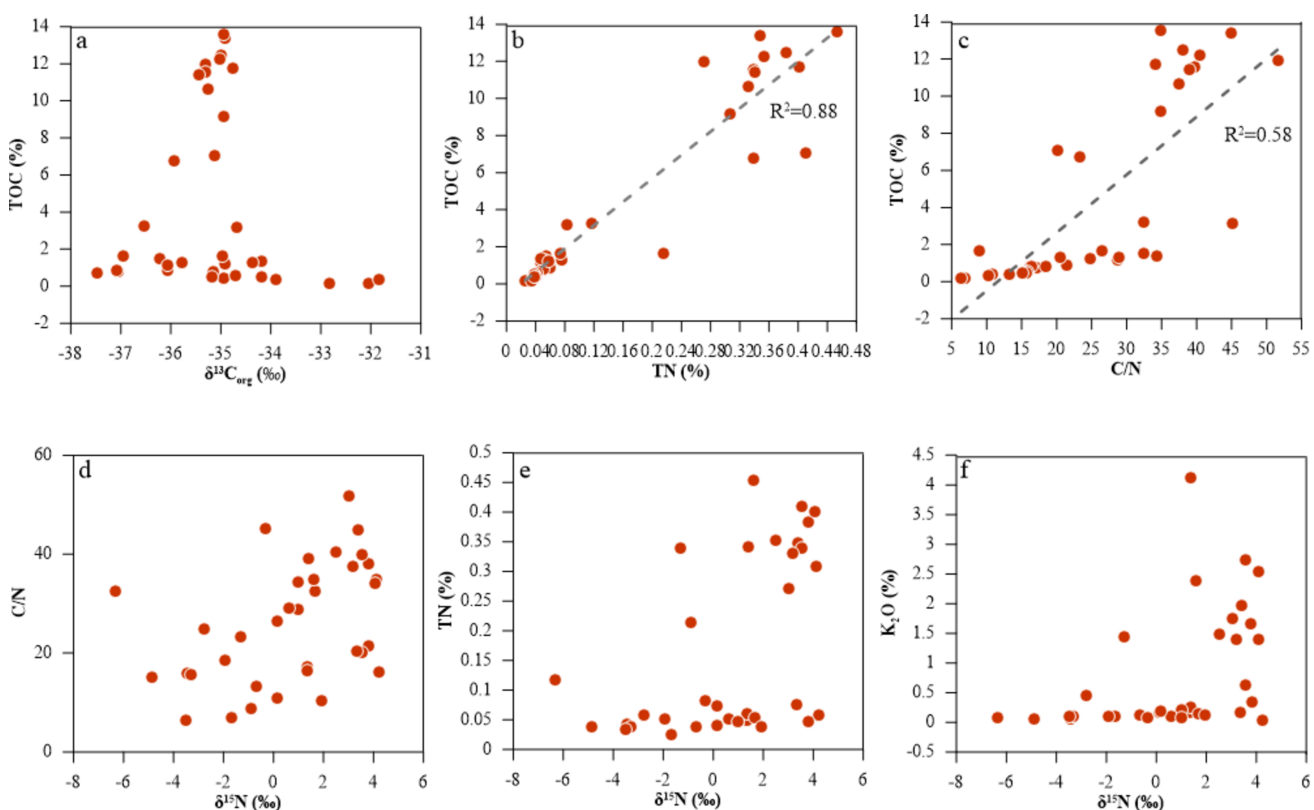


Fig. 5 Cross-plots of (a) TOC versus $\delta^{13}\text{C}_{\text{org}}$, (b) TOC versus TN, (c) TOC versus C/N, (d) C/N versus $\delta^{15}\text{N}$, (e) TN versus $\delta^{15}\text{N}$, and (f) K₂O versus $\delta^{15}\text{N}$ for the Yurtus Formation in the Shairike section

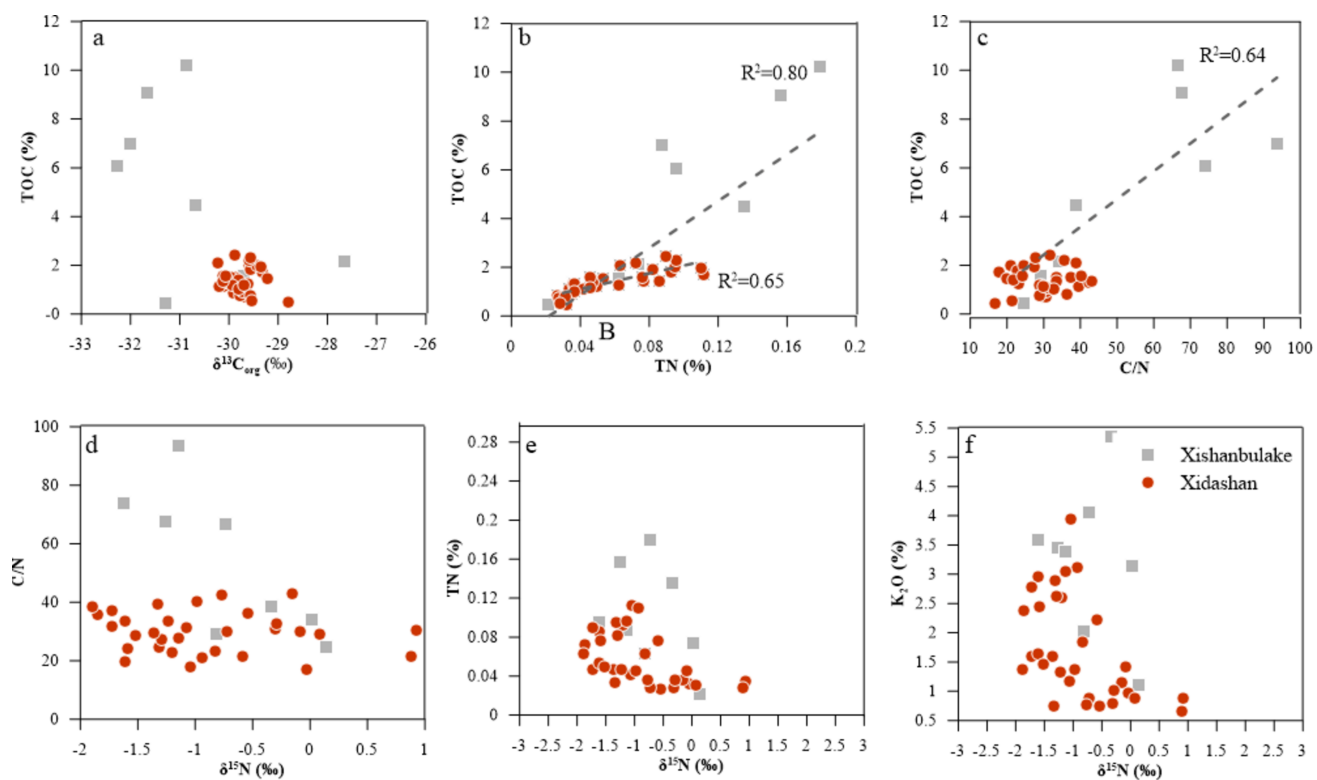


Fig. 6 Cross-plots of (a) TOC versus $\delta^{13}\text{C}_{\text{org}}$, (b) TOC versus TN, (c) TOC versus C/N, (d) C/N versus $\delta^{15}\text{N}$, (e) TN versus $\delta^{15}\text{N}$, and (f) K_2O versus $\delta^{15}\text{N}$ for the Xishanbulake and Xidashan Formations in Well Tadong 2

linear correlations for both the Xishanbulake and Xidashan Formations of Well Tadong 2 (Fig. 6b). These linear correlations indicate that the nitrogen mainly originated from organic matter, excluding a significant contribution of terrestrial non-primary nitrogen of the studied samples.

Oceanic phytoplankton is characterized by a mean C/N ratio of ca. 7 (Redfield et al. 1963). During the remineralization of organic matter, preferential loss of N would increase C/N ratios. For the Yurtus Formation at Shairike, the samples exhibit elevated C/N ratios of 6.4 to 51.6 (average = 25.9). The C/N ratios for the Xishanbulake and Xidashan Formations of Well Tadong 2 are 24.4 to 93.6 (average = 53.5) and 16.9 to 43.1 (average = 29.8), respectively. Linear correlations between TOC and C/N values are found in all studied units (Figs. 5c, 6c). The elevated C/N ratios of the studied units, along with the linear correlations in the TOC-C/N plots, may indicate partial loss of N during diagenesis and metamorphism in all studied units. The following section will explore the influence of diagenesis and metamorphism on the primary $\delta^{15}\text{N}$ of the studied samples.

Diagenetic processes can potentially alter the primary nitrogen isotopic signatures in sedimentary sequences (Stüeken et al. 2016). However, the changes in the primary $\delta^{15}\text{N}$ signatures vary depending on the redox conditions. In oxic settings, an increase in $\delta^{15}\text{N}$ values up to 4‰

accompanies by the release and subsequent oxidation of NH_4^+ in porewaters during diagenesis (Freudenthal et al. 2001; Lehmann et al. 2002). Moreover, oxic diagenesis is usually characterized by $\delta^{15}\text{N}$ values larger than 2‰ (Stüeken et al. 2016). In comparison, the isotopic fractionations in anoxic diagenetic processes are only minimal (< 2‰) (Freudenthal et al. 2001; Lehmann et al. 2002; Robinson et al. 2012). The samples from Well Tadong 2 were interpreted to have been deposited under a predominately anoxic setting based on the high enrichment of redox-sensitive elements (Guo et al. 2023). The anoxic diagenetic conditions, combined with all samples exhibiting $\delta^{15}\text{N} < 2\text{\textperthousand}$ (Table 2; Fig. 4), indicate that Well Tadong 2 samples are associated with anoxic diagenetic processes with minimal nitrogen isotopic alteration. Similarly, the Shairike samples, which were deposited in anoxic to euxinic water conditions (Zhu et al. 2022a), should have been subjected to minimal influences on the primary $\delta^{15}\text{N}$ signatures from diagenetic alteration.

Metamorphism during burial may also impose a significant effect on the primary nitrogen isotopic signatures of sedimentary successions. Thermal denitrogenation accompanied by metamorphism would lead to the preferential loss of ^{14}N , resulting in an increase in $\delta^{15}\text{N}$ (Ader et al. 2016). Previous studies show that the extent of $\delta^{15}\text{N}$ value change

differs among different metamorphic grades, with less than 2‰ for greenschist facies, 4‰ for amphibolite facies, and 6–10‰ for upper amphibolite phases (Bebout and Fogel 1992; Ader et al. 2016; Stüeken et al. 2017). According to previous studies in the Tarim Basin, the kerogen maturity of the Lower Cambrian successions from the Shairike section and Well Tadong 2 are still in the “gas window”, indicating the rocks are below the greenschist facies (Zhang et al. 2004; Wang 2021). Hence, metamorphic alteration on the $\delta^{15}\text{N}$ of our studied samples would be minimal.

Cross plots of $\delta^{15}\text{N-TN}$ and $\delta^{15}\text{N-C/N}$ also provide supporting evidence for the interpretation that diagenetic and metamorphic processes had negligible influences on the $\delta^{15}\text{N}$ values of our samples. As both processes are characterized by the loss of nitrogen and an increase in $\delta^{15}\text{N}$ values, negative correlations between $\delta^{15}\text{N-TN}$ and positive correlations between $\delta^{15}\text{N-C/N}$ would be expected for samples that subjected to significant alteration (Cremonese et al. 2014; Wang et al. 2015, 2018b; Ader et al. 2016). However, as shown in Figs. 5d, 5e and Figs. 6d, 6e, data points from all the studied units exhibit no evident $\delta^{15}\text{N-TN}$ and $\delta^{15}\text{N-C/N}$ correlations, indicating no significant alteration of the primary sedimentary $\delta^{15}\text{N}$ signatures. Also, no correlation is observed between potassium abundance and $\delta^{15}\text{N}$ (Figs. 5f; 6f), further demonstrating limited impact on nitrogen isotopes by diagenetic fluids (Zerkle et al. 2008).

5.2 Interpretation of nitrogen isotopic data

5.2.1 The Shairike section (northwestern Tarim)

As described in Sect. 4.1, the studied interval of the Yurtus Formation can be divided into two units according to the vertical profile in $\delta^{15}\text{N}$ values (Fig. 3). The $\delta^{15}\text{N}$ of the LU shows more variabilities, while the $\delta^{15}\text{N}$ of UU is more invariant. In the following text, the $\delta^{15}\text{N}$ signatures of the two units and their implications will be explored separately.

5.2.1.1 LU The $\delta^{15}\text{N}$ values for LU are highly variable, ranging from $-6.3\text{\textperthousand}$ to $4.2\text{\textperthousand}$ (average = $-0.2\text{\textperthousand}$) (Fig. 3). This unit is characterized by two pronounced negative excursions in $\delta^{15}\text{N}$ values, with nadirs of $-6.3\text{\textperthousand}$ and $-4.8\text{\textperthousand}$, respectively (Fig. 3). In addition to the highly negative values, there are also positive $\delta^{15}\text{N}$ values exceeding $+2\text{\textperthousand}$ within this interval (Fig. 3). The significant variability in $\delta^{15}\text{N}$ is similar to that of the Fortunian Liuchapo Formation at Yuanjia section in South China ($\delta^{15}\text{N}$: $-4.3\text{\textperthousand}$ to $+2\text{\textperthousand}$) (Wang et al. 2015), and is considered to reflect a shallow, unstable chemocline within water column during deposition, with strong upwelling regulating the nitrogen cycle within the water column (Ader et al. 2014; Wang et al. 2015). Such a scenario may also serve as a conceivable explanation for the highly variable $\delta^{15}\text{N}$ signatures

documented in the LU. The deposition of the Yurtus black rock series in northwest Tarim has been linked to a major transgression during the Early Cambrian (Yu et al. 2009; Zhang et al. 2020a; Zhu et al. 2022b). Accompanied by the transgression, widespread upwelling of deep anoxic waters was prevalent in this region, as indicated by geological and geochemical evidence including the presence of widespread phosphorite layers and nodules in the basal Yurtus Formation and the high Cd/Mo ratios typical of upwelling settings (Yu et al. 2009; Yang et al. 2017; Zhang et al. 2020a; Zhu et al. 2022a). In such circumstances, high primary productivity fueled by nutrient-rich, deep waters would cause enhanced respiratory oxygen demand in the water column (e.g., Yang et al. 2017; Zhang et al. 2020a). Meanwhile, the rise in sea level caused the impingement of anoxic waters to shallower depths (Harris et al. 2018). The combination of the two factors leads to a shoaling chemocline and further a reduction in the nitrate reservoir in shallow waters. According to such a scenario, ammonia traversing through the redox transition zone would reach the photic zone and be competitively assimilated or subjected to coupled denitrification and anammox, depending on the relative importance of the two processes (Ader et al. 2014, 2016). The former process that fractionates nitrogen isotopes by up to $-27\text{\textperthousand}$ would have been favored when upwelling was strong, generating negative $\delta^{15}\text{N}$ signatures (e.g., Higgins et al. 2012; Cremonese et al. 2014; Wang et al. 2015, 2018a; Chen et al. 2019). On the other hand, the dominance of the latter would drive the $\delta^{15}\text{N}$ signature towards positive values of $> 2\text{\textperthousand}$ due to the loss of ^{14}N during denitrification/anammox (Papineau et al. 2009; Godfrey et al. 2013; Ader et al. 2016; Chen et al. 2019). The instability of the redox transition zone would thereby generate $\delta^{15}\text{N}$ signatures with high variability ranging from negative to positive values (Ader et al. 2014), as observed in the LU.

Nitrogen fixation via the utilization of V- or Fe-based nitrogenase enzymes may also generate negative $\delta^{15}\text{N}$ values in sediments (Zhang et al. 2014; Stüeken et al. 2016). This process is known to occur exclusively in Mo-depleted conditions (Zhang et al. 2014). Nevertheless, studies on Fe-rich Archean and Proterozoic oceans, which presumably have even lower aqueous Mo in seawater than the Cambrian oceans, showed no convincing evidence to suggest that alternative V and/or Fe-based nitrogenases dominated N_2 -fixation (Stüeken et al. 2016; Chen et al. 2019). Moreover, a previous study showed the Mo/TOC ratios for the LU were higher than that of the UU, indicating higher levels of aqueous Mo in seawaters for the LU (Zhu et al. 2022a, b). If nitrogen fixation via the utilization of V- or Fe-based nitrogenase enzymes occurred during deposition, the UU would be more prone to showing negative $\delta^{15}\text{N}$ values. However, this study does not observe such negative $\delta^{15}\text{N}$ values in the UU (Fig. 3). Therefore, it is unlikely

that this process is responsible for the negative $\delta^{15}\text{N}$ values observed in the current study.

The $\delta^{13}\text{C}_{\text{org}}$ signatures of this interval are also consistent with a scenario with a shallow, unstable chemocline during a major transgression. Impingent of deeper, anoxic waters along with sea level rise and strong upwelling would have brought ^{12}C -rich inorganic carbon into the photic zone (e.g., Wang et al. 2015, 2018a, b). Subsequently, assimilation of the ^{12}C enriched carbon by organisms would produce light $\delta^{13}\text{C}_{\text{org}}$ values in the sedimentary record. The variabilities in $\delta^{13}\text{C}_{\text{org}}$ values, on the other hand, are reflective of the changes in the relative proportion of oxygenic photosynthetic biomass and anaerobic chemoautotrophic biomass in response to the instability in chemocline (e.g., Wang et al. 2018b).

5.2.1.2 UU The $\delta^{15}\text{N}$ values for the UU of the studied unit exhibit distinct characteristics in comparison to the LU. Except for the topmost interval, $\delta^{15}\text{N}$ values of most of this unit stay relatively invariant with $\delta^{15}\text{N}$ of $> 2\text{\textperthousand}$ (Fig. 3). Compared to the LU characterized by alternating anaerobic assimilation of NH_4^+ and denitrification/anammox, the less variable $\delta^{15}\text{N}$ values indicate a dominance of denitrification/anammox over partial ammonia assimilation. The reason underlying this transition in nitrogen cycle may be attributed to the decline of deep water upwelling. Marine sediments from settings with strong upwelling are usually characterized by high Cd/Mo ratios (Sweere et al. 2016). Thus, the lower Cd/Mo ratios in the UU likely indicates reduced upwelling intensities compared to the LU (Fig. 3) (Zhu et al. 2022a). The cessation of intense upwelling may have resulted in a deeper and more stable chemocline, enabling an expanded pool of NO_3^- in shallow waters and a shift towards denitrification/anammox dominating the nitrogen cycle in surface waters. Finally, the loss of bioavailable nitrogen via denitrification/anammox would leave the residual nitrogen pool ^{15}N -enriched, and subsequent biomass assimilating the residual NO_3^- in the photic zone acquired the isotopic signature with positive values $\delta^{15}\text{N}$ of $> 2\text{\textperthousand}$.

The uppermost of this unit is characterized by a shift in $\delta^{15}\text{N}$ towards lighter values within $-2\text{\textperthousand}$ to 1\textperthousand , which fall within the range typical of N_2 fixation via Mo-based nitrogenase (Ader et al. 2014; Stüeken et al. 2016). Since N_2 -fixation takes place when bioavailable nitrogen (nitrate and ammonia) is limited, the presence of N_2 -fixation signatures may indicate a shrink of the NO_3^- pool in shallow waters induced by intense denitrification and/or anammox. However, as only two samples were collected for this interval, the data may not have fully recorded the nitrogen isotopic signatures. The interpretation of N_2 fixation as a dominant nitrogen uptake pathway awaits further confirmation in future work.

Compared to the LU, the less variable $\delta^{13}\text{C}_{\text{org}}$ signatures of this unit are consistent with the stabilization of the chemocline during deposition. The $\delta^{13}\text{C}_{\text{org}}$ values are slightly higher than the highly negative values (as low as to $-37.5\text{\textperthousand}$) of LU, possibly due to a decline in upwelling intensities. Alternatively, the slightly higher values may reflect the enhancement of primary production relative to secondary (chemoautotrophic and/or methanotrophic) production to TOC.

5.2.2 Well Tadong 2 (eastern Tarim)

The $\delta^{15}\text{N}$ values in both the Xishanbulake and Xidashan Formations show limited variations, ranging from $-2\text{\textperthousand}$ to 1\textperthousand (Table 2; Fig. 4). The range and average $\delta^{15}\text{N}$ ($-0.7\text{\textperthousand}$ and $-0.9\text{\textperthousand}$ for the Xishanbulake and Xidashan Formation, respectively) of the two formations are similar, indicating no major changes in nitrogen cycling during deposition. There are two possible explanations for the $\delta^{15}\text{N}$ values throughout the studied interval. First, Mo-based N_2 fixation was the major nitrogen source for the local biota. In this case, limited isotopic fractionation imparted by this process would generate nitrogen isotopic signatures close to that of atmospheric N_2 ($\delta^{15}\text{N} = 0\text{\textperthousand}$) (Zerkle et al. 2008; Stüeken 2013; Ader et al. 2014). Second, an overall oxic seawater condition with denitrification entirely restricted to sediments could explain the near-zero $\delta^{15}\text{N}$ values. In this scenario, quantitative denitrification of nitrate would cause no isotopic fractionation, and the isotopic composition of nitrate assimilated by biomass would be close to that of fixed nitrogen (Algeo et al. 2014; Ader et al. 2016).

Both the Xishanbulake and Xidashan Formations of the Well Tadong 2 are highly enriched in Mo and U, with high Mo_{EF} and U_{EF} values indicative of predominately anoxic/euxinic bottom water conditions (Guo et al. 2023). Moreover, the Xishanbulake and Xidashan Formations from Well Tadong 1 with deeper water depth were also interpreted to have been deposited in anoxic bottomwater conditions (Guo 2023). The prevalence of anoxic bottom waters in the offshore sites suggests that the deep waters in the Tarim region during the Early Cambrian would have been anoxic. This indicates the seawater in the basin was likely redox-stratified similar to that of the Early Cambrian Nanhua Basin in South China (Jin et al. 2016; Li et al. 2020). A redox-stratified water column thus contradicts the scenario of a pervasively oxic ocean (i.e. the second scenario), which leaves N_2 fixation as the most plausible explanation for the observed $\delta^{15}\text{N}$ data. As the assimilation of molecular N_2 into organic matter takes place at the expense of high energy cost during the breakdown of the N–N bond, it dominates the ecosystem when other nitrogen species are at low concentrations (Karl et al. 2002; Sohm et al. 2011). The modern Black Sea serves as an excellent example of such a scenario, where the

extensive loss of bioavailable nitrogen (nitrate and ammonium) at the redox-transition zone hinders the accumulation of sufficient nitrate concentrations in surface waters, despite the high ammonium concentrations at depth (Ader et al. 2016). Collectively, the nitrogen isotopic signatures typical of N_2 fixation are compatible with a limited oceanic NO_3^- reservoir in a redox-stratified ocean in the Tarim Basin during the Early Cambrian.

The small fluctuations in $\delta^{15}\text{N}$ values in Well Tadong 2 may reflect the minor contribution of other nitrogen sources. Notably, concurrent negative excursions in $\delta^{15}\text{N}$ and $\delta^{13}\text{C}_{\text{org}}$ are observed at the lower part of the Xishanbulake Formation (Fig. 4). The $\delta^{13}\text{C}_{\text{org}}$ excursion has been reported before for the Well Tadong 2, and is considered to be correlated to the BACE excursion marking the basal Cambrian, which has been widely identified in different continental margins including the Yangtze platform (Wang et al. 2022). The incursion of ^{12}C -rich anoxic deep water into shallow waters linked to shoaling of chemocline and enhanced upwelling, accompanied by marine transgression, is invoked as the major mechanism responsible for the negative excursion (e.g., Wille et al. 2008; Chang et al. 2016; Wang et al. 2018a; Zhang et al. 2020b). Therefore, the synchronously negative excursion in both $\delta^{15}\text{N}$ and $\delta^{13}\text{C}_{\text{org}}$ may reflect the enhanced contribution of NH_4^+ assimilation in surface waters in response to increases in NH_4^+ and ^{12}C supplies via the influx of anoxic deep waters. In this case, NH_4^+ assimilation, which represents a subordinate nitrogen source, would be intensified, producing a small negative excursion in $\delta^{15}\text{N}$ values. Above the excursion, the $\delta^{15}\text{N}$ increases to ca 1 ‰ at the top of the Xishanbulake Formation. The increase coincides with a lithology transition from shale to limestone indicative of lower sea level (Fig. 4). The sea-level fall would lead to a deepening of chemocline, subsequently suppressing the contribution of NH_4^+ assimilation and promoting denitrification and/or anammox, thereby causing an increase in $\delta^{15}\text{N}$ values. (e.g., Ader et al. 2016; Hammarlund et al. 2017; Chang et al. 2019). The overlying Xidashan Formation is characterized by two negative excursions with comparable amplitude to that of the Xishanbulake Formation, while the $\delta^{13}\text{C}_{\text{org}}$ values stayed invariant. Similarly, the shifts towards higher $\delta^{15}\text{N}$ values are likely associated with lithological transitions suggestive of shallower water depths (Fig. 4). The small fluctuations can thus be readily explained by the same mechanism applied to the Xishanbulake Formation.

5.3 Implication for the Early Cambrian nitrogen cycle in the Tarim Basin

The two intervals studied in this research are not time-equivalent. The Xishanbulake and Xidashan Formations of Well Tadong 2 in eastern Tarim correspond to Fortunian to Stage 4, whereas the entire Yurtus Formation in northwestern

Tarim corresponds to Fortunian to lower Stage 3 (Sect. 2). The lack of paleontological data and radiometric age constraints pose challenges in correlating these two intervals. However, valuable insights can still be gained through analysis of the nitrogen isotopic signatures of the two sections.

Our data indicate significant differences in nitrogen cycling between the near-shore and off-shore sections when the black chert-shale of the Yurtus Formation was deposited (Fig. 7). In the near-shore Shairike section of northwestern Tarim Basin, our nitrogen isotope data demonstrated alternating anaerobic assimilation of NH_4^+ and denitrification/anammox in the shallow ocean during deposition of the LU. For the UU, with the reduction in upwelling intensity, nitrogen isotopic signatures featuring denitrification/anammox dominated. The nitrogen isotopic signatures of aerobic nitrogen cycling in the nearshore setting indicate at least a transient build-up of a local NO_3^- reservoir. By contrast, nitrogen signatures suggest persistent biological N_2 -fixation in the studied unit of the off-shore Well Tadong 2. As the studied interval of Well Tadong 2 encompasses the time interval of the entire Yurtus Formation at Shairike, the persistency of N_2 -fixation signatures of Well Tadong 2 indicates limited NO_3^- in the surface waters in the off-shore section during the deposition of the Yurtus black chert-shale. The observed spatial difference in nitrogen cycles is somewhat like the Mesoproterozoic ocean, where aerobic nitrogen cycle was restricted to nearshore settings whereas anaerobic nitrogen cycle dominated offshore environments (Stüeken 2013; Koehler et al. 2017). However, unlike the Precambrian Ocean with relatively low NH_4^+ concentrations (Stüeken et al. 2016), deep water with high concentrations of NH_4^+ may have been pervasive in the Early Cambrian Ocean due to widespread euxinic waters along continental margins. During organic matter remineralization via microbial sulfate reduction, organic nitrogen can be converted to NH_4^+ . As sulfate is not a strong enough oxidant to oxidize NH_4^+ , NH_4^+ can accumulate in euxinic settings, allowing its build-up to high concentrations at depth (e.g., Chen et al. 2019; Xu et al. 2020). In this case, strong upwelling of deep, NH_4^+ -rich waters would lead to enhanced NH_4^+ assimilation in coastal areas, generating highly negative $\delta^{15}\text{N}$ values as observed in the LU of the Shairike section.

Based on nitrogen isotopic data from a variety of sedimentary facies in South China, it has been proposed that the Early Cambrian witnessed the waxing and waning of the oceanic NO_3^- pool. Notably, a modern-like aerobic nitrogen cycle in response to the expansion of an oceanic NO_3^- reservoir was established in most of Fortunian and early Stage 3 (Wang et al. 2018a). If a large, stable NO_3^- pool also existed in the Tarim Basin during the Early Cambrian, sediments deposited in deep waters would be expected to exhibit high $\delta^{15}\text{N}$ values. Although data from Well Tadong 2 may not be fully representative of the evolution in nitrogen cycling

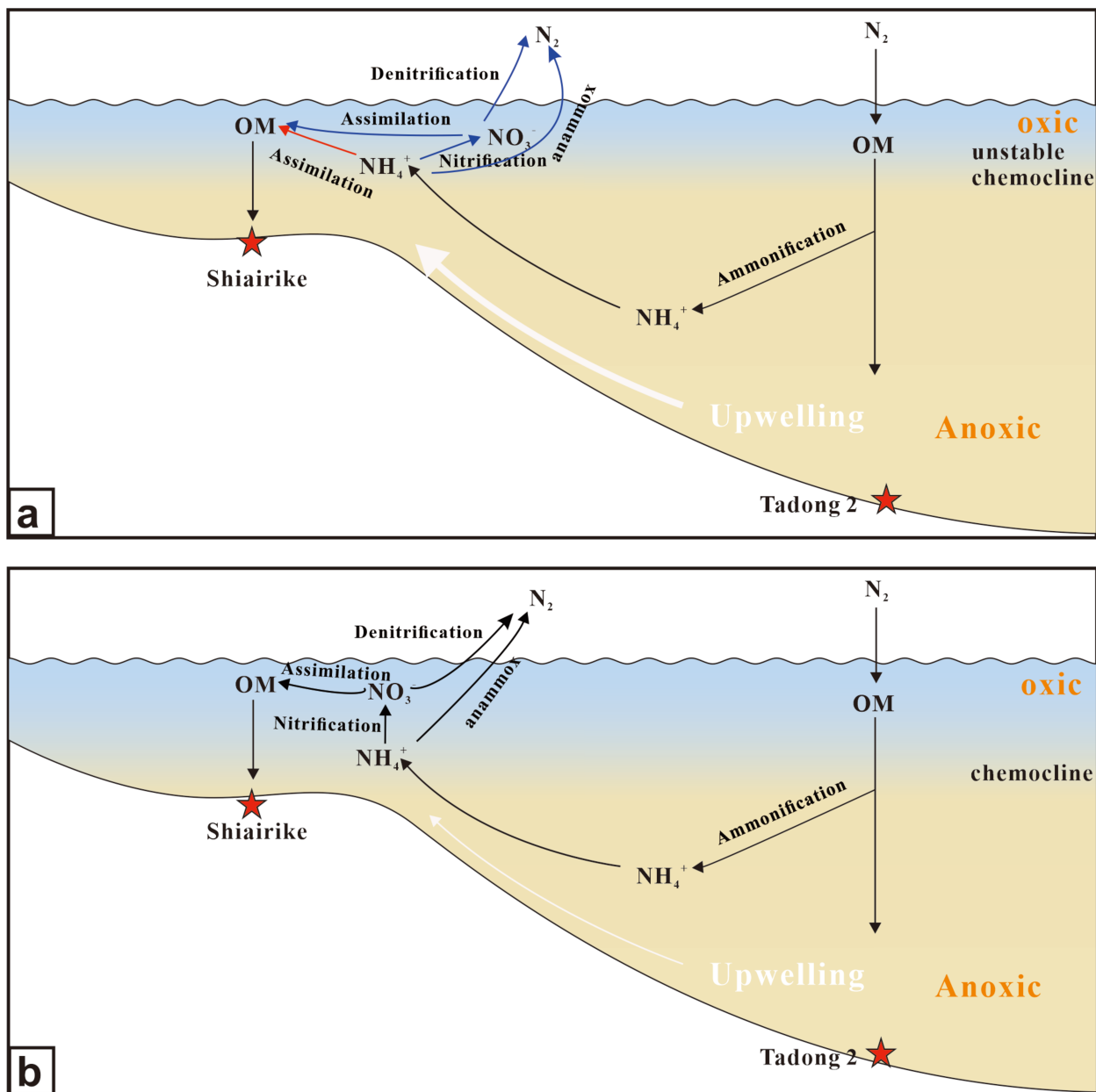


Fig. 7 Schematic diagram showing nitrogen cycle and ocean redox structure during deposition of the black shale-chert of Yurtus Formation. **a** Corresponds to the interval during which the LU was deposited. Red line: major nitrogen-cycling pathway when upwelling was strong; blue line: nitrogen-cycling pathway when upwelling was less intensive. **b** Corresponds to the interval when the UU was deposited

in the deep water regime of the Tarim Basin, the available data, which show nitrogen signatures typical of N_2 -fixation, seems to be more consistent with a scenario involving a limited nitrated reservoir in the basin when the Xishanbulake and Xidashan Formations were deposited (Fortunian to Age 4). This interpretation is not consistent with the model of episodic expansion of a large NO_3^- pool proposed by Wang et al. (2018a, b). The inconsistency may be attributed to (1) spatial heterogeneity in nitrogen cycling in different basins; (2) the Early Cambrian ocean is characterized by

a NO_3^- pool much smaller than proposed by Wang et al. (2018a, b). A recent compilation of nitrogen data from South China indicated that the build-up of NO_3^- reservoirs may have been only restricted to local settings during the Cambrian Age 3 (Xu et al. 2020), even during the peak of the Cambrian explosion (Chang et al. 2022). The new findings point to a scenario with a much smaller NO_3^- pool of the Early Cambrian ocean than that of the modern ocean; (3) It is also possible that sampling bias has led to the absence of highly positive $\delta^{15}N$ signatures. Nonetheless, a clearer

understanding of the nitrogen cycling pattern across the Tarim Basin and the global ocean during the Early Cambrian awaits future research involving a wider range of sedimentary facies from continental margins.

6 Conclusions

The present study presents paired $\delta^{15}\text{N}$ and $\delta^{13}\text{C}_{\text{org}}$ data from the Lower Cambrian Yurtus Formation of the Shairike section in the northwest Tarim Basin (inner ramp), as well as the Xishanbulake-Xidashan Formations in the eastern Tarim Basin (deep shelf/basin). Based on the data, the following information can be obtained.

The black chert-shale unit within the Yurtus Formation is characterized by a shoaling chemocline associated with upwelling and incursion of deep, anoxic waters during a transgression. The unit documented a shift in the nitrogen cycle processes. Specifically, the lower part of the unit exhibits highly variable $\delta^{15}\text{N}$ values, suggesting alternating dominance between anaerobic assimilation of NH_4^+ and denitrification/anammox, occurring against the backdrop of intense upwelling and an unstable chemocline. With the decrease in upwelling intensity, anaerobic assimilation of NH_4^+ weakened and denitrification/anammox began to dominate when the upper part was deposited. In contrast, the $\delta^{15}\text{N}$ values of the Xishanbulake and Xidashan Formations in the eastern Tarim Basin indicate that N_2 fixation served as the primary nitrogen source, while small fluctuations in $\delta^{15}\text{N}$ may reflect minor contributions from other nitrogen sources.

The two units investigated in the Shairike section and Well Tadong 2 are not temporally equivalent, as the latter encompasses a longer time interval. However, for the time interval when the black chert-shale unit of the Yurtus Formation at Shairike was deposited, spatial variation in the nitrogen cycle was observed in these sections, which aligns with an ocean characterized by redox stratification. The accumulation of a NO_3^- reservoir and aerobic nitrogen cycling in seawater primarily occurred in near-shore settings, while anaerobic nitrogen cycling, dominated by N_2 fixation, served as the main nitrogen uptake pathway in offshore environments.

Acknowledgements We thank Miss Liu Yang for her help in the lab. This project was financially supported by the Fundamental Research Funds for the Central Universities (No. B200202009).

Author's contribution Z.B. and Chen. Y-Q. designed the study. Z.B. and G.L. performed the research and wrote the paper. L.X-F conducted the chemical analyses and analyzed most of the data. All the authors contributed to refining the ideas and finalizing the paper.

Funding information Fundamental Research Funds for Central Universities of the Central South University, B200202009, Bi Zhu

Declarations

Conflict of interest On behalf of all authors, the corresponding author states that there is no conflict of interest.

References

- Ader M, Sansjofre P, Halverson GP et al (2014) Ocean redox structure across the Late Neoproterozoic Oxygenation Event: A nitrogen isotope perspective. *Earth Planet Sci Lett.* 396:1–13. <https://doi.org/10.1016/j.epsl.2014.03.042>
- Ader M, Thomazo C, Sansjofre P et al (2016) Interpretation of the nitrogen isotopic composition of Precambrian sedimentary rocks: Assumptions and perspectives. *Chem Geol.* 429:93–110. <https://doi.org/10.1016/j.chemgeo.2016.02.010>
- Algeo TJ, Meyers PA, Robinson RS et al (2014) Icehouse–greenhouse variations in marine denitrification. *Biogeosciences.* 11:1273–1295. <https://doi.org/10.5194/bg-11-1273-2014>
- Anbar AD, Knoll AH (2002) Proterozoic ocean chemistry and evolution: A bioinorganic bridge? *Science.* 297:1137–1142. <https://doi.org/10.1126/science.1069651>
- Bebout GE, Fogel ML (1992) Nitrogen-isotope compositions of meta-sedimentary rocks in the Catalina Schist, California: Implications for metamorphic devolatilization history. *Geochim Cosmochim Acta.* 56:2839–2849. [https://doi.org/10.1016/0016-7037\(92\)90363-N](https://doi.org/10.1016/0016-7037(92)90363-N)
- Boyle RA, Clark JR, Poulton SW et al (2013) Nitrogen cycle feedbacks as a control on euxinia in the mid-Proterozoic ocean. *Nat Commun.* 4:1533. <https://doi.org/10.1038/ncomms2511>
- Brasier MD (1992) Nutrient-enriched waters and the early skeletal fossil record. *J Geol Soc.* 149:621–629. <https://doi.org/10.1144/gsjgs.149.4.0621>
- Butterfield NJ (2018) Oxygen, animals and aquatic bioturbation: An updated account. *Geobiology.* 16:3–16. <https://doi.org/10.1111/gbi.12267>
- Cai Z, Xu Z, Tang Z et al (2011) The crustal deformation during the early Paleozoic period and the timing of orogeny in Kuruktag area on the northeast margin of Tarim Basin. *China Geol* 38:855–867 (CNKI:SUN:DIZI.0.2011-04-007 in Chinese with English abstract).
- Cai XY, Dou LW, Jiang HS (2014) Classification and correlation of Cambrian in eastern Tarim Basin. *Pet Geol Exp.* 5:539–545. [https://doi.org/10.11781/sysydz201405539. \(in Chinese with English abstract\)](https://doi.org/10.11781/sysydz201405539)
- Chang C, Hu W, Fu Q et al (2016) Characterization of trace elements and carbon isotopes across the Ediacaran-Cambrian boundary in Anhui Province, South China: Implications for stratigraphy and paleoenvironment reconstruction. *J Asian Earth Sci.* 125:58–70. <https://doi.org/10.1016/j.jseaes.2016.05.014>
- Chang C, Hu W, Wang X et al (2019) Nitrogen isotope evidence for an oligotrophic shallow ocean during the Cambrian Stage 4. *Geochim Cosmochim Acta.* 257:49–67. <https://doi.org/10.1016/j.gca.2019.04.021>
- Chang C, Wang Z, Huang KJ et al (2022) Nitrogen cycling during the peak Cambrian explosion. *Geochim Cosmochim Acta.* 336:50–61. <https://doi.org/10.1016/j.gca.2022.09.013>
- Chen X, Ling HF, Vance D et al (2015) Rise to modern levels of ocean oxygenation coincided with the Cambrian radiation of animals. *Nat Commun.* 6:7142. <https://doi.org/10.1038/ncomms8142>

- Chen Y, Diamond CW, Stüeken EE et al (2019) Coupled evolution of nitrogen cycling and redoxcline dynamics on the Yangtze Block across the Ediacaran-Cambrian transition. *Geochim Cosmochim Acta.* 257:243–265. <https://doi.org/10.1016/j.gca.2019.05.017>
- Cook PJ, Shergold JH (1984) Phosphorus, phosphorites and skeletal evolution at the Precambrian-Cambrian boundary. *Nature.* 308:231–236. <https://doi.org/10.1038/308231a0>
- Cremonese L, Shields-Zhou GA, Struck U et al (2014) Nitrogen and organic carbon isotope stratigraphy of the Yangtze Platform during the Ediacaran-Cambrian transition in South China. *Palaeogeogr Palaeoclimatol Palaeoecol.* 398:165–186. <https://doi.org/10.1016/j.palaeo.2013.12.016>
- Dong L, Xiao S, Shen B et al (2009) Basal Cambrian Microfossils from the Yangtze Gorges Area (South China) and the Aksu Area (Tarim Block, Northwestern China). *J Paleontol.* 83:30–44. <https://doi.org/10.1666/07-147R.1>
- Erwin DH, Laflamme M, Tweedt SM et al (2011) The Cambrian Conundrum: Early divergence and Later Ecological success in the early History of Animals. *Science.* 334:1091–1097. <https://doi.org/10.1126/science.1206375>
- Freudenthal T, Wagner T, Wenzhöfer F et al (2001) Early diagenesis of organic matter from sediments of the eastern subtropical Atlantic: evidence from stable nitrogen and carbon isotopes. *Geochim Cosmochim Acta.* 65:1795–1808. [https://doi.org/10.1016/S0016-7037\(01\)00554-3](https://doi.org/10.1016/S0016-7037(01)00554-3)
- Gao JF, Lu JJ, Lai MY et al (2003) Analysis of trace elements in rock samples using HR-ICPMS. *J Nanjing Univ Nat Sci.* 36:844–850 (in Chinese with English abstract).
- Godfrey LV, Poulton SW, Bebout GE et al (2013) Stability of the nitrogen cycle during development of sulfidic water in the redox-stratified Late Paleoproterozoic Ocean. *Geology.* 41:655–658. <https://doi.org/10.1130/G33930.1>
- Guo TT, Zhu B, Yang T et al (2023) Marine environmental evolution in the Early Cambrian, eastern Tarim Basin. *Pet Geol Exp.* 45:252–265.
- Guo TT (2023) Paleodepositional environment and organic matter accumulation of the Lower Cambrian Xishanbulake-Xidashan Formations in eastern Tarim Basin. Dissertation, Hohai University, Nanjing, China
- Hammarlund EU, Gaines RR, Prokopenko MG et al (2017) Early Cambrian oxygen minimum zone-like conditions at Chengjiang. *Earth Planet Sci Lett.* 475:160–168. <https://doi.org/10.1016/j.epsl.2017.06.054>
- Harris NB, McMillan JM, Knapp LJ et al (2018) Organic matter accumulation in the Upper Devonian Duvernay Formation, Western Canada Sedimentary Basin, from sequence stratigraphic analysis and geochemical proxies. *Sediment Geol.* 376:185–203. <https://doi.org/10.1016/j.sedgeo.2018.09.004>
- He T, Zhu M, Mills BJW et al (2019) Possible links between extreme oxygen perturbations and the Cambrian radiation of animals. *Nat Geosci.* 12:468–474. <https://doi.org/10.1038/s41561-019-0357-z>
- Higgins MB, Robinson RS, Husson JM et al (2012) Dominant eukaryotic export production during ocean anoxic events reflects the importance of recycled NH_4^+ . *Proc Natl Acad Sci USA.* 109:2269–2274. <https://doi.org/10.1073/pnas.1104313109>
- Jin C, Li C, Algeo TJ et al (2016) A highly redox-heterogeneous ocean in South China during the Early Cambrian (~529–514 Ma): Implications for biota-environment co-evolution. *Earth Planet Sci Lett.* 441:38–51. <https://doi.org/10.1016/j.epsl.2016.02.019>
- Karl D, Michaels A, Bergman B et al (2002) Dinitrogen fixation in the world's oceans. *Biogeochemistry.* 57:47–98. <https://doi.org/10.1023/A:1015798105851>
- Kipp MA, Stüeken EE, Yun M et al (2018) Pervasive aerobic nitrogen cycling in the surface ocean across the Paleoproterozoic Era. *Earth Planet Sci Lett.* 500:117–126. <https://doi.org/10.1016/j.epsl.2018.08.007>
- Knoll AH (2017) Food for early animal evolution. *Nature.* 548:528–530. <https://doi.org/10.1038/nature23539>
- Knoll AH, Follows MJ (2016) A bottom-up perspective on ecosystem change in Mesozoic oceans. *Proc R Soc B.* 283:20161755. <https://doi.org/10.1098/rspb.2016.1755>
- Koehler MC, Stüeken EE, Kipp MA et al (2017) Spatial and temporal trends in Precambrian nitrogen cycling: A Mesoproterozoic offshore nitrate minimum. *Geochim Cosmochim Acta.* 198:315–337. <https://doi.org/10.1016/j.gca.2016.10.050>
- Lehmann MF, Bernasconi SM, Barbieri A, McKenzie JA (2002) Preservation of organic matter and alteration of its carbon and nitrogen isotope composition during simulated and in situ early sedimentary diagenesis. *Geochim Cosmochim Acta.* 66:3573–3584. [https://doi.org/10.1016/S0016-7037\(02\)00968-7](https://doi.org/10.1016/S0016-7037(02)00968-7)
- Li ZX, Powell CM (2001) An outline of the palaeogeographic evolution of the Australasian region since the beginning of the Neoproterozoic. *Earth-Sci Rev.* 53:237–277. [https://doi.org/10.1016/S0012-8252\(00\)00021-0](https://doi.org/10.1016/S0012-8252(00)00021-0)
- Li ZX, Bogdanova SV, Collins AS et al (2008) Assembly, configuration, and break-up history of Rodinia: A synthesis. *Precambrian Res.* 160:179–210. <https://doi.org/10.1016/j.precamres.2007.04.021>
- Li C, Cheng M, Zhu M et al (2018) Heterogeneous and dynamic marine shelf oxygenation and coupled early animal evolution. *Emerging Top Life Sci.* 2:279–288. <https://doi.org/10.1042/ETLS20170157>
- Li C, Shi W, Cheng M et al (2020) The redox structure of Ediacaran and Early Cambrian oceans and its controls. *Sci Bull.* 65:2141–2149. <https://doi.org/10.1016/j.scib.2020.09.023>
- Mills DB, Canfield DE (2014) Oxygen and animal evolution: Did a rise of atmospheric oxygen “trigger” the origin of animals? *BioEssays.* 36:1145–1155. <https://doi.org/10.1002/bies.201400101>
- Papineau D, Purohit R, Goldberg T et al (2009) High primary productivity and nitrogen cycling after the Paleoproterozoic phosphogenic event in the Aravalli Supergroup, India. *Precambrian Res.* 171:37–56. <https://doi.org/10.1016/j.precamres.2009.03.005>
- Peng S, Babcock LE, Cooper RA (2012) The Cambrian Period. In: *The geologic time scale.* Elsevier, Amsterdam, pp 437–488
- Qian Y, Feng WM, Li GX et al (2009) Taxonomy and biostratigraphy of the Early Cambrian univalved mollusc fossils from Xinjiang. *Acta Micropalaentol Sin.* 26(3):193–210 (in Chinese with English abstract).
- Redfield AC, Ketchum BH, Richards FA (1963) The influence of organisms on the composition of sea-water. *Sea* 2:26–77
- Robinson RS, Kienast M, Luiza Albuquerque A et al (2012) A review of nitrogen isotopic alteration in marine sediments. *Paleceanography.* 27:2012PA002321. <https://doi.org/10.1029/2012PA002321>
- Sohm JA, Webb EA, Capone DG (2011) Emerging patterns of marine nitrogen fixation. *Nat Rev Microbiol* 9:499–508. <https://doi.org/10.1038/nrmicro2594>
- Sperling EA, Stockey RG (2018) The temporal and environmental context of early animal evolution: Considering all the ingredients of an “Explosion.” *Integr Comp Biol.* 58:605–622. <https://doi.org/10.1093/icb/icy088>
- Sperling EA, Frieder CA, Raman AV et al (2013) Oxygen, ecology, and the Cambrian radiation of animals. *Proc Natl Acad Sci USA.* 110:13446–13451. <https://doi.org/10.1073/pnas.1312778110>
- Stüeken EE (2013) A test of the nitrogen-limitation hypothesis for retarded eukaryote radiation: Nitrogen isotopes across a Mesoproterozoic basinal profile. *Geochim Cosmochim Acta.* 120:121–139. <https://doi.org/10.1016/j.gca.2013.06.002>
- Stüeken EE, Kipp MA, Koehler MC et al (2016) The evolution of Earth's biogeochemical nitrogen cycle. *Earth-Sci Rev.* 160:220–239. <https://doi.org/10.1016/j.earscirev.2016.07.007>
- Stüeken EE, Zaloumis J, Meixnerová J, Buick R (2017) Differential metamorphic effects on nitrogen isotopes in kerogen extracts and bulk rocks. *Geochim Cosmochim Acta.* <https://doi.org/10.1016/j.gca.2017.08.019>

- Sweere T, Van Den Boorn S, Dickson AJ, Reichart G-J (2016) Definition of new trace-metal proxies for the controls on organic matter enrichment in marine sediments based on Mn, Co, Mo and Cd Concentrations Chem Geol. 441:235–245. <https://doi.org/10.1016/j.chemgeo.2016.08.028>
- Tian L, Cui HF, Liu J et al (2018) Early-Middle Cambrian paleogeography and depositional evolution of Tarim Basin. Oil Gas Geol. 39(5):1011–1021. <https://doi.org/10.11743/ogg20180515> (in Chinese with English abstract).
- Wang D, Struck U, Ling HF et al (2015) Marine redox variations and nitrogen cycle of the Early Cambrian southern margin of the Yangtze Platform, South China: Evidence from nitrogen and organic carbon isotopes. Precambrian Res. 267:209–226. <https://doi.org/10.1016/j.precamres.2015.06.009>
- Wang D, Ling HF, Struck U et al (2018a) Coupling of ocean redox and animal evolution during the Ediacaran-Cambrian transition. Nat Commun. 9:2575. <https://doi.org/10.1038/s41467-018-04980-5>
- Wang X, Jiang G, Shi X et al (2018b) Nitrogen isotope constraints on the Early Ediacaran ocean redox structure. Geochim Cosmochim Acta. 240:220–235. <https://doi.org/10.1016/j.gca.2018.08.034>
- Wang Z, Chang C, Zhang X et al (2021) Possible response of N₂O emission to marine redox fluctuation during the Ediacaran-Cambrian transition in Nanhua Basin. South China Precambrian Res. 365:106409. <https://doi.org/10.1016/j.precamres.2021.106409>
- Wang H, Su J, Wang X et al (2022) Carbon isotope stratigraphy of the Cambrian System in the Eastern Tarim Basin. China Acta Geol Sin (Engl Ed). 96:1277–1293. <https://doi.org/10.1111/1755-6724.14972>
- Wang HK (2021) Source rocks sedimentary environment and hydrocarbon generating potential of the Lower Cambrian in Kalpin thrust belt. Dissertation, China University of Petroleum, Beijing
- Wei GY, Planavsky NJ, Tarhan LG et al (2018) Marine redox fluctuation as a potential trigger for the Cambrian explosion. Geology. 46:587–590. <https://doi.org/10.1130/G40150.1>
- Wille M, Nägler TF, Lehmann B et al (2008) Hydrogen sulphide release to surface waters at the Precambrian/Cambrian boundary. Nature. 453:767–769. <https://doi.org/10.1038/nature07072>
- Xiang L, Schoepfer SD, Zhang H et al (2018) Evolution of primary producers and productivity across the Ediacaran-Cambrian transition. Precambrian Res. 313:68–77. <https://doi.org/10.1016/j.precamres.2018.05.023>
- Xu D, Wang X, Shi X et al (2020) Nitrogen cycle perturbations linked to metazoan diversification during the Early Cambrian. Palaeogeogr Palaeoclimatol Palaeoecol. 538:109392. <https://doi.org/10.1016/j.palaeo.2019.109392>
- Yang ZY, Luo P, Liu B et al (2017) The difference and sedimentation of two black rock series from Yurtus Formation during the Earliest Cambrian in the Aksu area of Tarim Basin. Northwest China Acta Petrol Sin. 33(6):1893–1918 (in Chinese with English abstract).
- Yao J, Xiao S, Yin L et al (2005) Basal Cambrian microfossils from the Yurtus and Xishanblaq formations (Tarim, north-west China): Systematic revision and biostratigraphic correlation of micrhystridium-like acritarchs: Basal cambrian microfossils. Palaeontology. 48:687–708. <https://doi.org/10.1111/j.1475-4983.2005.00484.x>
- Yu B, Yu L, Chen J et al (2003) The suboxic depositional setting of black shales in Lower Cambrian from northern Tarim Basin. Earth Sci Front. 10:545–550. <https://doi.org/10.3321/j.issn:1005-2321.2003.04.020> (in Chinese with English abstract).
- Yu B, Dong H, Widom E et al (2009) Geochemistry of basal Cambrian black shales and cherts from the Northern Tarim Basin, Northwest China: Implications for depositional setting and tectonic history. J Asian Earth Sci. 34:418–436. <https://doi.org/10.1016/j.jseas.2008.07.003>
- Zerkle AL, Junium CK, Canfield DE et al (2008) Production of 15 N-depleted biomass during cyanobacterial N₂-fixation at high Fe concentrations. J Geophys Res. 113:2007JG000651. <https://doi.org/10.1029/2007JG000651>
- Zhang SG (1983) Early Cambrian Archaeocyathids from Kuruktag, Xinjiang. Acta Palaeont Sin. 22:9. <https://doi.org/10.19800/j.cnki.aps.1983.01.002>. (in Chinese with English abstract)
- Zhang X, Shu D (2014) Causes and consequences of the Cambrian explosion. Sci China Earth Sci. 57:930–942. <https://doi.org/10.1007/s11430-013-4751-x>
- Zhang SC, Wang ZM, Wang FY et al (2004) oil accumulation history in Tadong 2 oil reservoir in Tarim Basin, NW China-A case study of oil stability and cracking. Petr Pet Explor Dev. 31(6):25–31 (in Chinese with English abstract).
- Zhang CL, Zou HB, Li HK et al (2013) Tectonic framework and evolution of the Tarim Block in NW China. Gondwana Res. 23:1306–1315. <https://doi.org/10.1016/j.gr.2012.05.009>
- Zhang X, Sigman DM, Morel FMM et al (2014) Nitrogen isotope fractionation by alternative nitrogenases and past ocean anoxia. Proc Natl Acad Sci USA. 111:4782–4787. <https://doi.org/10.1073/pnas.1402976111>
- Zhang G, Liu W, Zhang L et al (2015) Cambrian-Ordovician prototypic basin, paleogeography and petroleum of the Tarim craton. Earth Sci Front. 22:269–276. <https://doi.org/10.13745/j.esf.2015.03.023>. (in Chinese with English abstract)
- Zhang J, Fan T, Zhang Y et al (2017) Heterogenous oceanic redox conditions through the Ediacaran-Cambrian boundary limited the metazoan zonation. Sci Rep. 7:8550. <https://doi.org/10.1038/s41598-017-07904-3>
- Zhang C, Guan S, Wu L et al (2020a) Depositional environments of Early Cambrian marine shale, northwestern Tarim Basin, China: Implications for organic matter accumulation. J Pet Sci Eng. 194:107497. <https://doi.org/10.1016/j.petrol.2020.107497>
- Zhang X, Zhou X, Hu D (2020b) High-resolution paired carbon isotopic records from the Meishucun section in South China: Implications for carbon cycling and environmental changes during the Ediacaran-Cambrian transition. Precambrian Res. 337:105561. <https://doi.org/10.1016/j.precamres.2019.105561>
- Zhong D, Hao Y (1990) Sinian to Permian Stratigraphy and Palaeontology of the Tarim Basin, Xinjiang, (I) Kuruktag Region (in Chinese). Nanjing University Press, Nanjing
- Zhou ZY (2001) Stratigraphy of the Tarim Basin (in Chinese). Science Press, Beijing.
- Zhou Z, Chen P (1990) Biostratigraphy and Geological Evolution of Tarim (in Chinese). Science Press, Beijing
- Zhu ZL, Lin HL (1983) Some Early Cambrian trilobites from the Xidashan Formation of Kuruktag, Xinjiang. Acta Palaeontol Sin. 22:22–30. <https://doi.org/10.19800/j.cnki.aps.1983.01.003>. (in Chinese with English abstract).
- Zhu MY, Yang AH, Yuan J et al (2019) Cambrian integrative stratigraphy and timescale of China. Sci China Earth Sci. 62:25–60. <https://doi.org/10.1007/s11430-017-9291-0>
- Zhu MY, Sun ZX, Yang AH et al (2021) Lithostratigraphic subdivision and correlation of the Cambrian in China. J Stratigr. 45(3):223–249. <https://doi.org/10.19839/j.cnki.dcxzz.2021.0022>
- Zhu B, Yang T, Wang J et al (2022a) Multiple controls on the paleoenvironment of the Early Cambrian black shale-chert in the northwest Tarim Basin, NW China: Trace element, iron speciation and Mo isotopic evidence. Mar Pet Geol. 136:105434. <https://doi.org/10.1016/j.marpgeo.2021.105434>
- Zhu G, Li T, Zhao K et al (2022b) Mo isotope records from Lower Cambrian black shales, northwestern Tarim Basin (China): Implications for the Early Cambrian ocean. Geol Soc Am Bull. 134:3–14. <https://doi.org/10.1130/B35726.1>

Springer Nature or its licensor (e.g. a society or other partner) holds exclusive rights to this article under a publishing agreement with the author(s) or other rightsholder(s); author self-archiving of the accepted manuscript version of this article is solely governed by the terms of such publishing agreement and applicable law.